Preliminary Design and Simulation of a Thermal Management System with Integrated Secondary Power Generation Capability for a Mach 8 Aircraft Concept Exploiting Liquid

*aerospace*

MDPI

*Article*

# Preliminary Design and Simulation of a Thermal Management System with Integrated Secondary Power Generation Capability for a Mach 8 Aircraft Concept Exploiting Liquid Hydrogen

**Davide Ferretto * and Nicole Viola**

Department of Mechanical and Aerospace Engineering, Politecnico di Torino, 10129 Torino, Italy
* Correspondence: davide.ferretto@polito.it

**Abstract:** This paper introduces the concept of a thermal management system (TMS) with integrated on-board power generation capabilities for a Mach 8 hypersonic aircraft powered by liquid hydrogen (LH2). This work, developed within the EU-funded STRATOFLY Project, aims to demonstrate an opportunity for facing the challenges of hypersonic flight for civil applications, mainly dealing with thermal and environmental control, as well as propellant distribution and on-board power generation, adopting a highly integrated plant characterized by a multi-functional architecture. The TMS concept described in this paper makes benefit of the connection between the propellant storage and distribution subsystems of the aircraft to exploit hydrogen vapors and liquid flow as the means to drive a thermodynamic cycle able, on one hand, to ensure engine feed and thermal control of the cabin environment, while providing, on the other hand, the necessary power for other on-board systems and utilities, especially during the operation of high-speed propulsion plants, which cannot host traditional generators. The system layout, inspired by concepts studied within precursor EU-funded projects, is detailed and modified in order to suggest an operable solution that can be installed on-board the reference aircraft, with focus on those interfaces impacting its performance requirements and integration features as part of the overall systems architecture of the plane. Analysis and modeling of the system is performed, and the main results in terms of performance along the reference mission profile are discussed.

**Keywords:** thermal management system; on-board power generation; hypersonic aircraft; regenerative cooling; liquid hydrogen; on-board system simulation



**Citation:** Ferretto, D.; Viola, N. Preliminary Design and Simulation of a Thermal Management System with Integrated Secondary Power Generation Capability for a Mach 8 Aircraft Concept Exploiting Liquid Hydrogen. *Aerospace* **2023**, *10*, 180. https://doi.org/10.3390/aerospace10020180

Academic Editor: Hao Xia

Received: 29 December 2022
Revised: 3 February 2023
Accepted: 9 February 2023
Published: 14 February 2023



## 1. Introduction

Thermal management is a well-known critical aspect for enabling hypersonic flight [1], especially when this regime is sustained over long mission time, as within the typical trajectory profile of cruise and acceleration vehicles (CAVs) [2] involved in point-to-point transport operations in the stratosphere. This issue is even more relevant when vehicle configurations exploit slender layouts, being conceived, on one hand, to enhance aerodynamic efficiency in cruise but, on the other hand, experiencing higher heat fluxes, particularly in leading edge areas. The selection of a suitable concept for the aforementioned mission, in terms of high-level requirements associated with Mach number and cruise altitude, is in fact evidenced to have a considerable impact on the accumulated heat load as well. This can be a key aspect to drive the selection of the most effective thermal control strategy [3]. Together with aerodynamic heating, heat also comes from internal sources, such as high-speed propulsion plants, on-board systems and the payload, that can play a significant role on the overall heat exchange process among the different parts of the aircraft. In case the vehicle is supposed to host passengers, the global thermal management System (TMS) of the aircraft should also be properly interfaced with an environmental control plant, responsible for maintaining pressure, temperature and chemical air mixture within

acceptable limits inside the cabin compartments [4]. The use of cryogenic fluids, potentially integrated with the powerplant itself, which exploits them as propellant, provides an interesting advantage to the thermal control problem. In fact, species such as the liquid hydrogen (LH2) are characterized by very low operating temperatures and very good thermal properties, as far as heat exchange and heat sinks processes are concerned, together with a high energy per unit mass. Several examples of thermodynamic cycles benefiting from the use of cryogenic fluids are available in the literature [5–7], proposing different strategies to deal with thermal management issues of different vehicle configurations. The concepts actively linked to the propulsion plant, i.e., exploiting the actual propellant as the means of coolant for critical aircraft areas, appear very promising, since they do not need additional fluids to properly work. These strategies allow for reducing the inert mass of the vehicle and offer, as consequence, the highest volumetric efficiency to host the payload. However, integration with the overall on-board systems architecture should be carefully assessed, since the working cycle of such a TMS cannot be analyzed without looking at propellant system behavior. As a matter of fact, the mass flow of the fluid is a direct consequence of powerplant needs, also considering that propellant consumption is subjected to specific depletion sequences to keep the center of gravity (CoG) of the aircraft within operational limits. In turn, maintaining the CoG within the design limit may contribute to reducing control surface deflections to trim the vehicle, also limiting trim drag [8]. This means that, for CAVs, integration of on-board systems with the overall vehicle is a key aspect for defining an effective and efficient product concept. Ultimately, on-board power generation can be considered as an additional constraint, since high-speed propulsion systems, mainly characterized by ramjet/scramjet architectures, are not suitable to host conventional generators. Thus, finding alternative ways to produce electrical and/or hydraulic power on-board is another issue that can be tackled with integrated thermal and energy management systems [9–13].

Taking into account the aforementioned issues, this paper introduces the concept of a TMS with integrated on-board power generation capabilities for the STRATOFLY MR3 vehicle [14], a Mach 8 hypersonic aircraft powered by liquid hydrogen. This concept was studied within the homonymous project with the aim of demonstrating the possibility of reaching a Technology Readiness Level (TRL) of enabling technologies for high-speed flight up to level 6 by 2035 [15]. This by defining a technology roadmap with a process similar to those developed for space exploration case studies [16]. After this brief introduction, Section 2 evaluates the relevant literature studies in the field of thermal management for high-speed vehicles, with focus on the exploitation of advanced thermodynamic cycles. Then, Section 3 presents the reference vehicle and mission to be used as starting point for development of the TMS, which is thoroughly described in Section 4, which is where system modeling and simulation are presented and the main results are discussed. Section 5 draws major conclusions, paving the way to potential future works on this specific system concept.

## 2. Studies on Advanced Thermodynamic Cycles for Thermal Management of High-Speed Vehicles

As already anticipated in Section 1, while looking at thermal management systems (TMSs) for high-speed vehicles, several examples of thermodynamic cycles are available in the literature, providing at least theoretical results and insights on the effectiveness of different solutions. The main focus of most of the works is dedicated to the powerplant, which may require a relevant number of resources to ensure a proper cooling of critical parts, such as the combustor and nozzle. In this context, [5] shows that a traditional regenerative cooling architecture for the thermal management of a scramjet engine can be less efficient than a closed Brayton cycle (CBC), since, in the latter case, the heat sink capability of cryogenic fuel, such as hydrogen, can be increased. Additionally, the energy collected by the fuel itself, used as the main coolant of the cycle, can be transformed into work to generate auxiliary power. This work highlights how the simple regenerative cooling

process introduces considerable irreversible losses because of the temperature difference between the fluid and the heated surfaces, while the use of an active cycle may reduce this temperature differential, enhancing the thermal efficiency of the process. On the other hand, when looking at the entire vehicle, different approaches dealing with the management of the whole thermal network on-board can also be used as reference. Particularly, [6] shows how a careful design of active cooling networks (ACNs) can be crucial to reach an efficient design of a thermal protection system (TPS) for a Mach 8 vehicle, benefiting from the advantage of active cooling combined with passive cooling in different parts of the aircraft. In this case, a storable propellant was used, demonstrating the flexibility of the approach and the possibility of customizing the network for the specific areas to be protected, depending on the local heat fluxes to be tackled. However, in order to increase the heat exchange capabilities of the process, analyses on different fluids can also be found, as proposed in [7]. Here, supercritical nitrogen is proposed as the main means of coolant for a quite complex TMS architecture designed to support hypersonic flight. This concept treats the fluid as expendable, and it was conceived to manage heat coming from aerodynamic heating, powerplant, cabin and on-board systems. This cycle is capable of interfacing a main loop, where the supercritical nitrogen is provided to different users, as well as dedicated closed loops depending on the users themselves that can use also different fluids for local cooling. At the end of the process, the nitrogen is blown away after cooling the powerplant and the TPS through transpiration cooling. However, in this case, this work focuses on the derivation of a more accurate model for the prediction of fluid characteristics rather than focusing on the cycle itself, even if the main idea is very much in line with the scope of this work. Another concept for the integrated cooling of the overall aircraft exploiting liquid hydrogen both as propellant and means of coolant can be found in [9], where the energies embedded in the fluid can also be used to generate secondary power, guaranteeing the self-sustainability of the active cycle, as well as potentially offering a power source for other users. This concept is thus known as the thermal and energy management system (TEMS) and it was analyzed within the frame of the Long-term Advanced Propulsion Concepts and Technologies II (LAPCAT II) [17] and HIKARI Projects [9]. The cycle proposed in [9] aims to use the liquid portion of hydrogen within a regenerative cooling process of the propulsion plant, while boil-off generated within the tanks can be adopted for airframe and on-board systems cooling, with potential interface with the environmental control system (ECS) of the cabin, as also demonstrated in [4]. In this case, the heated hydrogen of the regenerative branch can then be expanded through a turbine, driving both the dedicated fuel pump and the boil-off compressor similarly to what was suggested in [5]. An excess of power from this process is expected to be in the MW class, potentially offering a substantial power off-take especially in scramjet-powered flight phases, where traditional engine-mounted generators cannot be used. As far as power generation is concerned, other concepts may use more complex architectures, interfacing a fuel-based cooling cycle with liquid metal powerplant cooling, exploiting an advanced electromagnetic pumping process, as shown in [10]. In fact, liquid metals have been found to be effective means for cooling small areas characterized by high heat fluxes, such as thin scramjet walls or leading edges, through both active and passive solutions such as heat pipes [18]. In this case, the cycle is made up of a closed recuperative Brayton (CRB) architecture with three loops: a first fuel loop for a preliminary heating before injection in the combustion chamber, a helium loop as the intermediate cycle between fuel and liquid metal, and the final liquid sodium cycle. The CRB cycle is actually embedded within the helium loop, where the turbine used to expand the fluid can guarantee a power off-take of about 130 kW in peak condition. Most of the available concepts therefore make use of energy transfer from fluidic sources to mechanical and electrical targets, but works such as [11] propose the adoption of a thermo-electric generator (TEG) to support a CBC architecture. In this case, the whole architecture is similar to the one proposed by [10], but a three-stages TEG is selected to support powerplant cooling of a similar configuration. This cycle uses nitrogen as the primary loop, a helium loop for the CBC, and a final methane loop feeding the TEG and the powerplant itself. The results

show that the power peak potentially generated by the adoption of the coupled CBC-TEG architecture is around 650 kW. A similar power generation class solution is proposed in [12], where a concept for a power and thermal management system (PTMS) for a long-endurance hypersonic vehicle (Mach 6–7) is described. In this case, supercritical carbon dioxide (SCO2) is used within a CBC to exchange heat with fuel in order to produce a thermal cracking reaction. This allows for the exploiting of pyrolysis vapor of fuel for the expansion within a dedicated turbine before entering the combustion chamber, also producing electrical power. The SCO2 then enters a compressor before being injected within the cooling jacket of the powerplant and, in turn, is then expanded while exiting from this channel to produce additional power. The authors highlight that this dual generation system is more effective than the simple CBC, being capable of producing up to 200 kW for a typical Mach 7 mission, with a total mass of the system of about 2000 kg. The concept is then optimized within [13], with reference to minimum fuel weight penalty and minimum heat sink consumption of fuel as optimization objectives. Details on the fuel-SCO2 heat exchanger are provided, with reference to printed circuit heat exchanger (PCHE) architecture. The enhanced and optimized cycle can even increase its power generation capability up to MW class with reduced mass.

As a final remark, then, it is possible to say that considerable difference among the architectures is mainly associated with complexity, availability of fluids on-board and power generation capability when considering similar vehicle classes and mission types. For the purpose of this work, the TEMS concept proposed by [9] was taken as reference, considering the beneficial re-use of hydrogen boil-off and the relatively simple architecture still providing, at least theoretically, a MW class secondary power. Additionally, the similarity of the case study eases the system definition process, even if an effective implementation of the plant on-board the aircraft still needs to be found in order to make the system operable, as described in Section 4.1. This is actually an issue for all the aforementioned approaches, since a theoretical representation of the cycle is often present, but advice or details on how to practically implement the cycle on-board are often not specified (e.g., number of elements, redundancy issues, distance among elements and location on the aircraft, etc. ... ). Moreover, an insight on the influence of the TMS operational cycle on propellant plant and consumption, also with reference to CoG shift, is highlighted. For these reasons, this work aims to focus on the aforementioned aspects, as shown in the next sections. In addition, in order to reduce the complexity associated with the modeling and simulation of such a kind of system, the proposed TMS concept (Section 4) takes into account powerplant cooling only, even if still considers interfaces with the cabin environmental control system (ECS) as an example of external utility (other than the propellant system, whose interface is a pre-requisite for enabling the TMS). Airframe thermal control is instead not included within the analysis, even if theoretically applicable to the concept.

## 3. The STRATOFLY MR3 Hypersonic Cruiser

From the configuration standpoint, the STRATOFLY MR3 aircraft (Figure 1) follows the layout proposed by LAPCAT II Project for its MR2.4 vehicle [17], with some differences. It is still characterized by a waverider architecture, with a dorsal-mounted propulsion plant duct, a canard and a V-Tail layout for directional stability and control. The main differences between the MR2.4 and MR3 external layouts are related to the overall dimensions, which are slightly extended for the MR3; the shape of the V-Tail; and the upper part of the aft section of the nozzle, as well as the introduction of additional control surfaces (nozzle flaps). The integration of the propulsive system at the top of the vehicle allows for maximizing the available planform area for lift generation without additional drag penalties, thus increasing the aerodynamic efficiency (up to a maximum value in a cruise of about 7), and it allows for optimizing the internal volume. Specifically, STRATOFLY MR3 integrates six air turbo rocket engines, ATR, that operate up to Mach 4–4.5 (available thrust at sea level 233 kN for each engine), and one dual-mode ramjet, DMR, that is used for hypersonic flight

from Mach 4.5 up to Mach 8 (available thrust 664 kN in cruise). The powerplant flow path is shown in Figure 2 for what concerns the complete ATR-DMR arrangements. As can be seen, the high-speed flow path feeding the DMR (red) is the main duct of the powerplant, allowing the flow to pass through the overall vehicle from the intake (gray) to the final common nozzle (blue). ATR ducts are instead grouped in two assemblies (green) on both sides of the main DMR duct (three engines per side). These are fed by opening a portion of the intake up to Mach 4–4.5, whose gap can be modulated depending on the flow field. The DMR duct is instead composed by the intake and an isolator, followed by a combustor and the nozzle, which is divided into two segments (one dedicated exclusively to the DMR, followed by the common nozzle, where exhaust flow coming from the ATR is also injected).

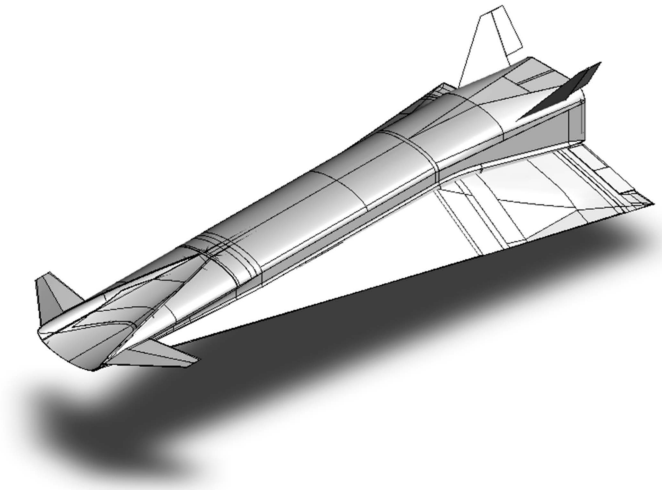

**Figure 1.** STRATOFLY MR3 layout.

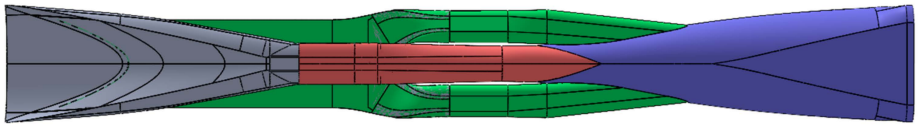

**Figure 2.** STRATOFLY MR3 propulsive flow path.

The external dimensions are characterized by an overall length of 94.7 m (excluding protruding rudders) and by a wingspan of 41.1 m. The planform area (excluding canards) is thus around 2517 $m^2$ with an overall internal volume arrangement of roughly 10,000 $m^3$.

This aircraft is conceived to carry 300 passengers over antipodal routes up to around 18,000 km, flying at an average altitude of 30–35 km at Mach 8. The expected maximum take-off weight (MTOW) is around 400,000 kg, with a total propellant mass of about 180,000 kg of liquid hydrogen (LH2) and a design payload mass of 33,000 kg.

The results of the reference trajectory simulation, i.e., the Brussels to Sydney mission [19], implemented using the ASTOS software, show that the overall flight can be completed with a total travel time of 3 h 24 min. An overview of the complete trajectory in terms of altitude and Mach profiles of the vehicle are reported in Figure 3. The propellant mass variation over time is shown in Figure 4a. The thrust and mass flow profiles are reported in Figure 4b for the ATR (continuous line) and DMR (dotted line).

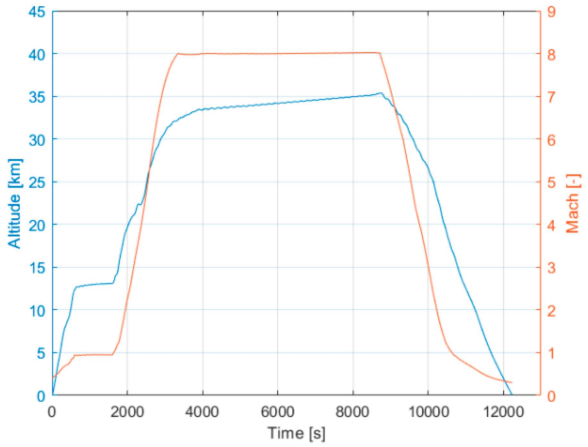


**Figure 3.** STRATOFLY MR3 mission profile in terms of altitude and Mach number as function of time [19].

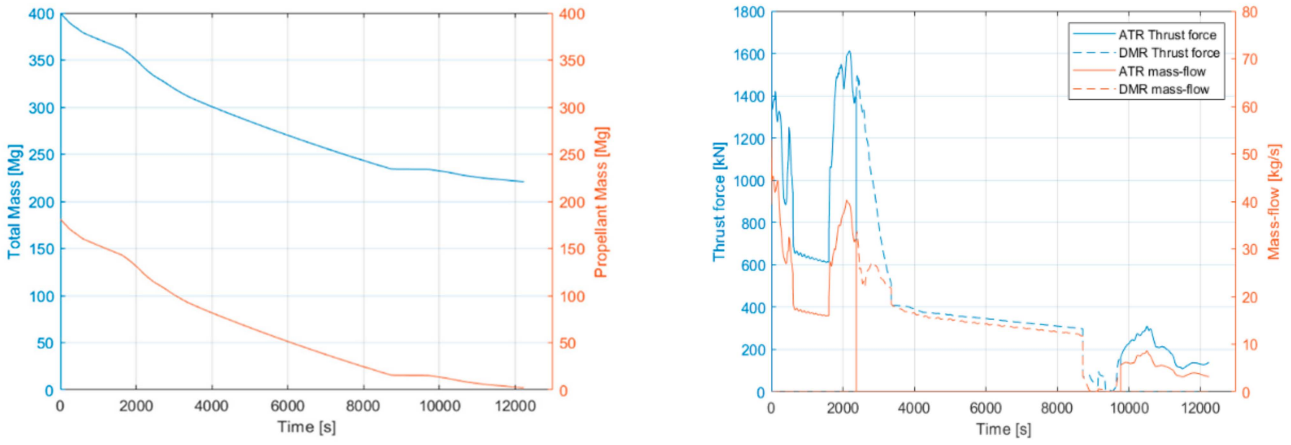


(**a**) (**b**)

**Figure 4.** STRATOFLY MR3 propellant mass (**a**), engine thrust (total) and propellant mass flow (**b**) as function of time [20].

The propellant subsystem is in fact one of the most impactful plants on-board the STRATOFLY MR3 vehicle, since the use of LH2 requires a large amount of volume that is dedicated to tanks and delivery lines. The overall tank architecture (Figure 5) is made up of seven main assemblies (front additional tank—FAT including sub-compartments front intake—FI, front part—FP, middle front part—MFP, middle part—MP, middle rear part—MRP and rear part—RP, then front pillow tank—FPT, rear pillow tank—RPT, front wing tank—FWT, center wing tank—CWT, rear wing tank—RWT and wing tip tank—WTT). These vessels are sized in terms of volume and thicknesses (both structural and insulation) [20] in order to propose a feasible bubble layout, distributing structural loads and offering a good compromise between center of gravity (CoG) control during flight and thermal management needs. The vehicle is able to host 2000 $m^3$ of LH2 (85% tank efficiency) corresponding to 180,000 kg of fluid in case of a density equal to 90 $kg/m^3$ (with a temperature of 13 K).

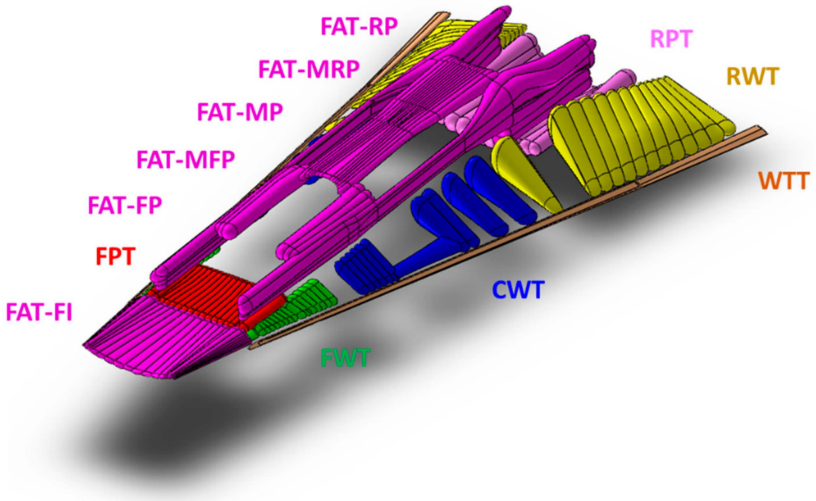


**Figure 5.** STRATOFLY MR3 LH2 tank architecture [20].

## 4. A Thermal Management System with Integrated Power Generation Capabilities for STRATOFLY MR3

### *4.1. System Architecture Description*

The principle behind the TEMS concept, as already studied in LAPCAT II [17] and HIKARI [9], is based on the use of hydrogen, which is present on-board primarily as propellant, not only to cool down critical aircraft areas and powerplant elements, but also as a means to generate secondary power. As already anticipated in Section 2, the original concept [9] exploited LH2 within a regenerative cooling cycle to cool down powerplant elements (especially combustion chambers and the nozzle through a cooling jacket architecture) using the fluid from the engine feed line. This concept is particularly interesting since it does not require additional fluids, such as helium, nitrogen or others, potentially saving on overall system mass because of the absence of other circuits and tanks. This also allows for maintaining a rather simple working cycle if compared to [10,12]. This fluid, pumped through dedicated components, is then heated and subsequently expanded through a turbine before injection within the combustor. On the other hand, the boil-off produced within the LH2 tanks can be used, in parallel, as an additional coolant means for other elements of the aircraft (such as ECS heat exchangers, cabin, etc. . . . ) after being compressed through a dedicated machine driven by the LH2 turbine. An excess of power generated through expansion within the turbine can be used for other on-board needs. The STRATOFLY MR3 TMS concept has a similar architecture, being based on the same physical phenomena. The main differences with the work performed in [9] are related to the implementation of the plant on the aircraft, with focus on the connection with the distributed propellant system. As consequence, a detailed analysis on the depletion sequence of the tanks as a function of the needs of the propulsion plant all along the mission, analyzed in [20], drove the layout definition and modeling of the updated TMS architecture. In fact, a higher level of detail was devoted to the operational configuration in order to implement a feasible solution within the aircraft, overcoming a purely theoretical concept and sketching the interfaces with the new on-board subsystems network. Moreover, it is important to highlight that the overall propellant plant was re-designed for the STRATOFLY MR3 vehicle, since the original cabin layout proposed in [17] for the LAPCAT MR2.4 concept was dropped and updated with a new one [4] characterized by a shorter length and an easier rectangular planform shape. This introduced a different volume allocation on-board the aircraft, and the overall tank network was deeply updated, reaching a substantial difference between MR3 and MR2.4 propellant compartment breakdown, both in terms of practical shape and hierarchy.

The basic cycle of the updated TMS is reported in Figure 6. As can be seen, the LH2 line (blue) is used within the regenerative cooling cycle on the powerplant, collecting LH2

from auxiliary tanks (through transfer pumps), delivering it to the primary tank and then delivering it to the dedicated engine cooling jackets. After heating, the fluid is expanded through a turbine that cools down the hydrogen, also setting the correct injection pressure, and produces power to drive other TMS utilities, as well as feed other on-board subsystems if required. Main pumping assembly can be driven by the TMS turbine itself, considering the high-power demand [20]. The boil-off line (cyan) is instead dedicated to the cooling of other utilities and loads. Gaseous hydrogen (H2) is collected from the different tanks and compressed in order to be injected within a dedicated cycle. The boil-off compressor is driven by the LH2 turbine. Once the boil-off has concluded its cycle, it is injected within the powerplant by mixing with the LH2 line after the turbine.

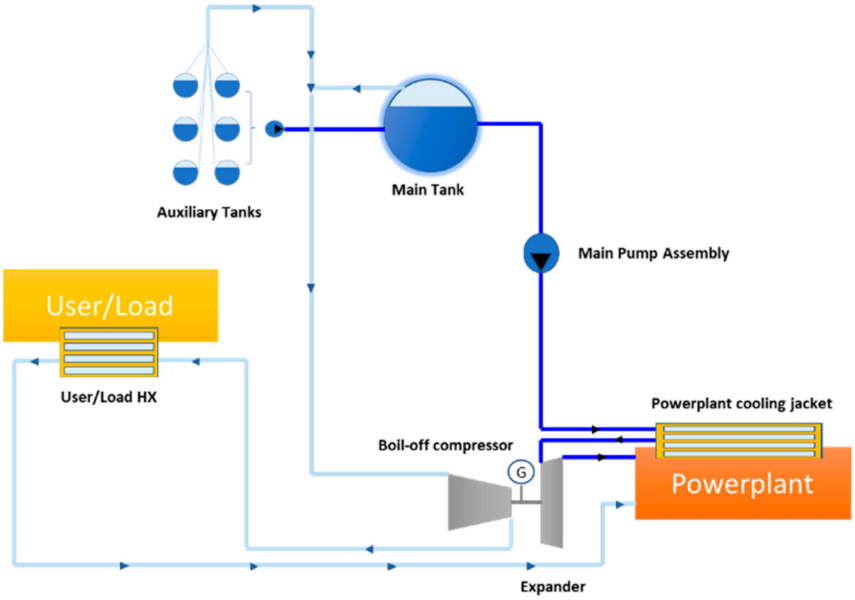


**Figure 6.** STRATOFLY MR3 thermal management system architecture [20].

The presence of the TMS is crucial for the operational feasibility of the vehicle concept. In fact, there is no other possibility to produce secondary power on-board during high-speed phases, when the powerplant is based on ramjet/scramjet operation of the DMR. Additionally, the TMS can also be exploited for lower-speed flight, since it can also be theoretically operated with ATR if engines are running, reducing the power bleed from the powerplant and, as a consequence, reducing the fuel consumption. This is also a considerable benefit of TMS operation, since the boil-off fraction, which is usually a negative effect of cryogenic circuits, is used and re-injected within the powerplant without wasting the precious and expensive hydrogen [21,22]. This additionally increases the fuel efficiency, reducing the fraction of fuel consumption that is not directly related to powerplant performance. In order to allocate this TMS concept on-board and connect it to the operational modes of other subsystems, such as, for example, the ECS and the propellant subsystem, a dedicated analysis was carried out to translate the theoretical cycle in a implemented schematic. In fact, considering the layout of the aircraft and, particularly, the propellant depletion sequence defined in [20], the TMS was divided in three modules, as shown in Figure 7.

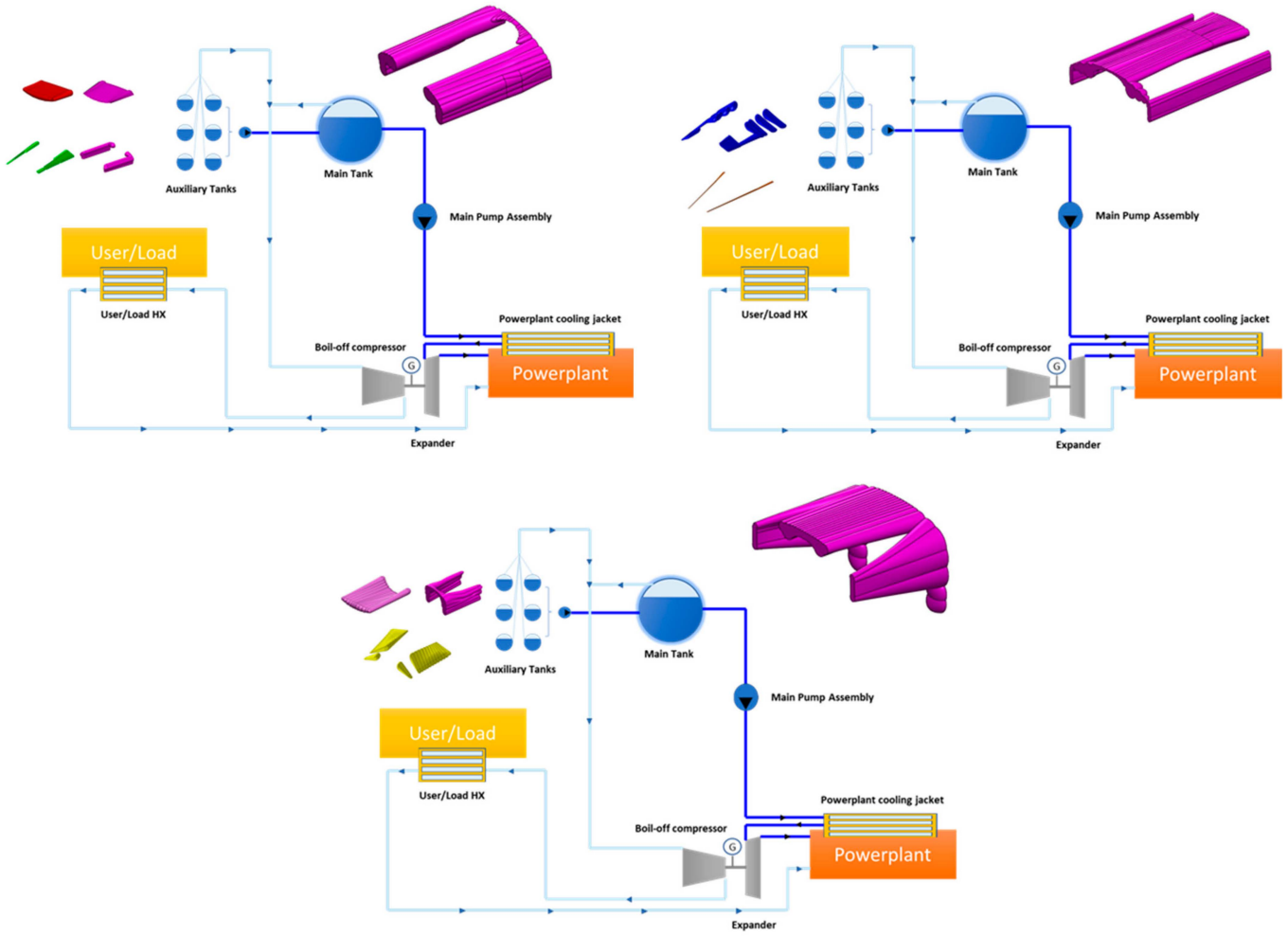


**Figure 7.** Thermal management system modules.

This subdivision is necessary to allow connection of TMS with the three different primary tanks (and related auxiliary propellant compartments, represented within the top left corner of the different sub-figures). This guarantees a complete coverage of mission phases in terms of cooling and power generation capabilities, considering that the delivery line is active to guarantee nominal operation of the plant. At the same time, all modules are connected to the main users, such as the ECS and the powerplant cooling jacket, in order to ensure seamless operation during the switch between one module and another one (for example, when the associated primary tank is completely empty). Moreover, the presence of different modules may allow for the enhancement of operational safety, since possible failures, especially within delivery lines, leading to cooling or power generation problems can be balanced by other modules of the TMS. Additionally, the different modules, depending on their position on-board (front part, middle part, aft part of the aircraft) can deal with local utilities requirements in terms of cooling and offer a more flexible solution for real-life implementation on-board in comparison to the single plant, which can be difficult to install in one shot.

### *4.2. Assumptions on Systems Interfaces with Impact on TMS Performance*

#### 4.2.1. Interface Heat Fluxes

In order to set the most relevant boundary conditions to assess the effectiveness and the feasibility of the system, it is necessary to start by considering the primary function of the TMS, i.e., thermal control. For the purpose of this analysis, except from the interface with the ECS (Section 4.2.4), only powerplant-related thermal loads are considered. Thanks

to CFD evaluations performed in [23], it was possible to predict the heat fluxes produced by the DMR combustion process, which were expected to be around $4 MW/m^2$ in the chamber, while the DMR nozzle was subjected to lower fluxes (about $1 MW/m^2$). Downstream, after ATR exhaust flow injection, the remaining part of the common nozzle received an average flux of $500 kW/m^2$.

#### 4.2.2. Powerplant Geometrical Interfaces

The extension of protection by means of cooling jacket includes part of the combustor (from hydrogen injector position towards downstream), the DMR nozzle and part of the common nozzle. This means that the assembly including the combustor and common nozzle is around 15 m, while 39 m out of 42 for the common nozzle are equipped with the cooling jacket. The overall dimensions are shown within Figure 8. The sections view represents the DMR combustor (constant section) and the interface between the DMR nozzle outlet and common nozzle inlet, as well as the common nozzle towards the outlet (where protection ends).

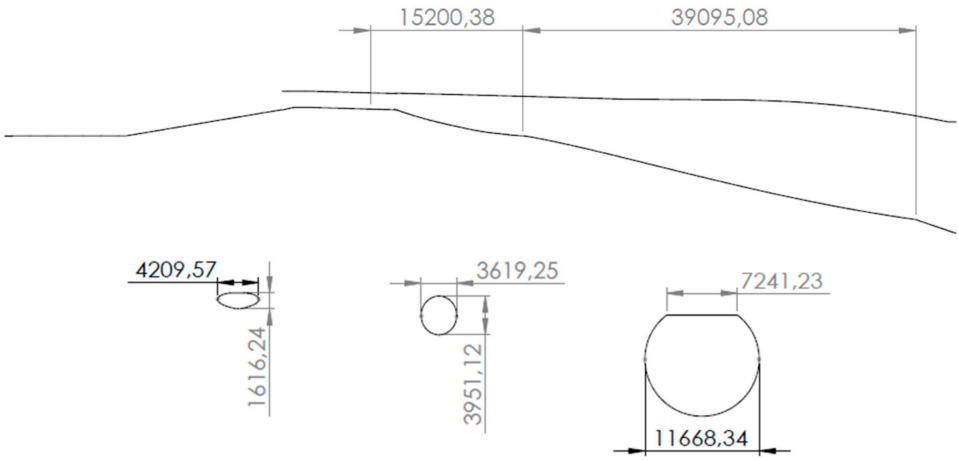


**Figure 8.** Extension of protected powerplant surfaces (mm).

The design of the geometrical features of the cooling jacket, originally proposed by [24] and reviewed in [25], led to the layout shown in Figure 9 for the first exchanger (similar for the second one).

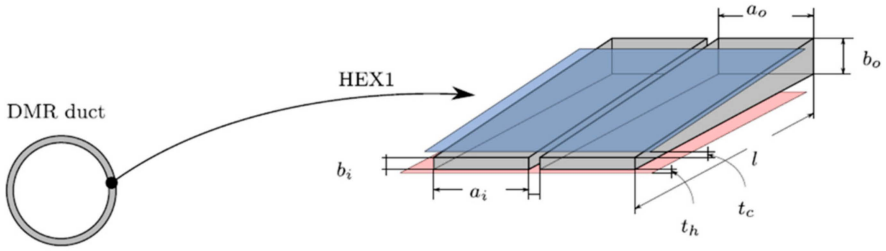


**Figure 9.** Exchanger layout [19].

For the combustor and the DMR nozzle, each segment has an average width $(a)$ of about 0.004 m and an average height $(b)$ of about 0.0015 m, linearly spaced between 9 sections. The common nozzle is protected in a similar way, but the average dimension of segment width is about 0.50 m and the height is around 0.010 m.

#### 4.2.3. Propellant System Interfaces

The hydrogen flow actually drives the overall process, so it is important to evaluate the mass flow rate available within the circuit. This cannot be chosen independently from powerplant needs, since propellant consumption is directly associated with the

required thrust that the engines provide. Thus, LH2 flow is a function of the specific fuel consumption of the powerplant all along the mission, being considerably variable. On the other hand, boil-off levels are also associated with the equilibrium of the fluid within the tanks, and gaseous hydrogen flow is also not constant. For the purpose of this study, the considered propellant mass flow is shown in Figure 3, while the boil-off rate was assumed to be 10% of the liquid portion to take into account tank thermal equilibrium. Considering the similarities with the work performed in [9] and as a consequence of the thermal interfaces specified in Section 4.2.1, a resulting interface temperature on the propulsion plant cooling jacket side was determined (Section 4.4), as also suggested by [3]. In turn, the thermal management of tanks was based on a passive solution by introducing a proper insulation layer to protect propellant compartments. The vehicle aeroshell as well as powerplant flow path were conceived to be made of ceramic matrix composite (CMC) material, while the tank structural layer was made of aluminum. The insulation layer for each tank was selected according to the preliminary model suggested by [26], where the thickness of the layer can be computed according to the property of the fluid within the compartments, the interface temperature, the insulation material characteristics and the exposition period (according to the mission specified in Section 3), as in (1).

$$t_{ins} = \sqrt{\frac{k_{ins} t_{flight} \left(T_{int} - T_{fluid}\right)}{h_{fuel}\, \rho_{fuel}}} \tag{1}$$

where

$\rho_{fuel}$ is the density of propellant [kg/m$^3$];
$k_{ins}$ is the conductivity of insulation material [W/(m K)];
$t_{flight}$ is flight time [s];
$T_{int}$ is the temperature of the compartments adjacent to the tank (internal to the vehicle) [K];
$T_{fluid}$ is the temperature of the liquid inside the tank [K];
$h_{fuel}$ is the heat of vaporization of the fuel [J/kg].

This led to the determination of an insulation layer between 10 to 20 cm of silica aerogel (0.003 W/(m K) conductivity), depending on the tank location, shape and thickness of the structural layer. For what concerns mechanical stress, the fluid in the tanks is supposed to be stored at 20 K and 0.1 MPa, while boil-off temperature is supposed around 80 K. The pressure at the inlet of the fuel control unit of the powerplant, (outlet of feeding line turbine) was set at 6 MPa, according to the hypotheses of [9]. This tank layout was then parametrized within the simulation environment in order to obtain consistent variable trends. Additionally, the tank depletion sequence has a large influence on TMS module activation, since, depending on the actual primary tank that is feeding the powerplant, different parts of the TMS layout can be running. In fact, as shown in Sections 4.3 and 4.4, the TMS working cycle was analyzed separately for the three modules, while global performance could only be evaluated at the end of the process. TMS module activation depended on the availability of LH2 flow within the primary feeding line of the main tanks, which in turn was related to the depletion strategy of auxiliary tanks. For these reasons, modules could be alternatively activated along the mission profile, according to the sequence specified in [20]. This was done not only to take into account cooling needs (the necessary amount of propellant should be kept within the compartments that are closer to the areas that need thermal control/protection) but also to keep aircraft CoG within prescribed ranges in order to reduce control surface deflections required to trim the aircraft (reducing the trim drag and enhancing the aerodynamic efficiency). As a consequence, the LH2 flow rates shown in Figure 10 directly provide insight into this activation sequence for the three modules. In fact, where flow was present, the related module was active (there was no overlap among the modules in nominal conditions). The first module to be activated was the one fed by the tanks positioned on the aft side of the aircraft (to bring

CoG forward during the first phases of the flight). Then, the different modules followed the prescribed sequence.

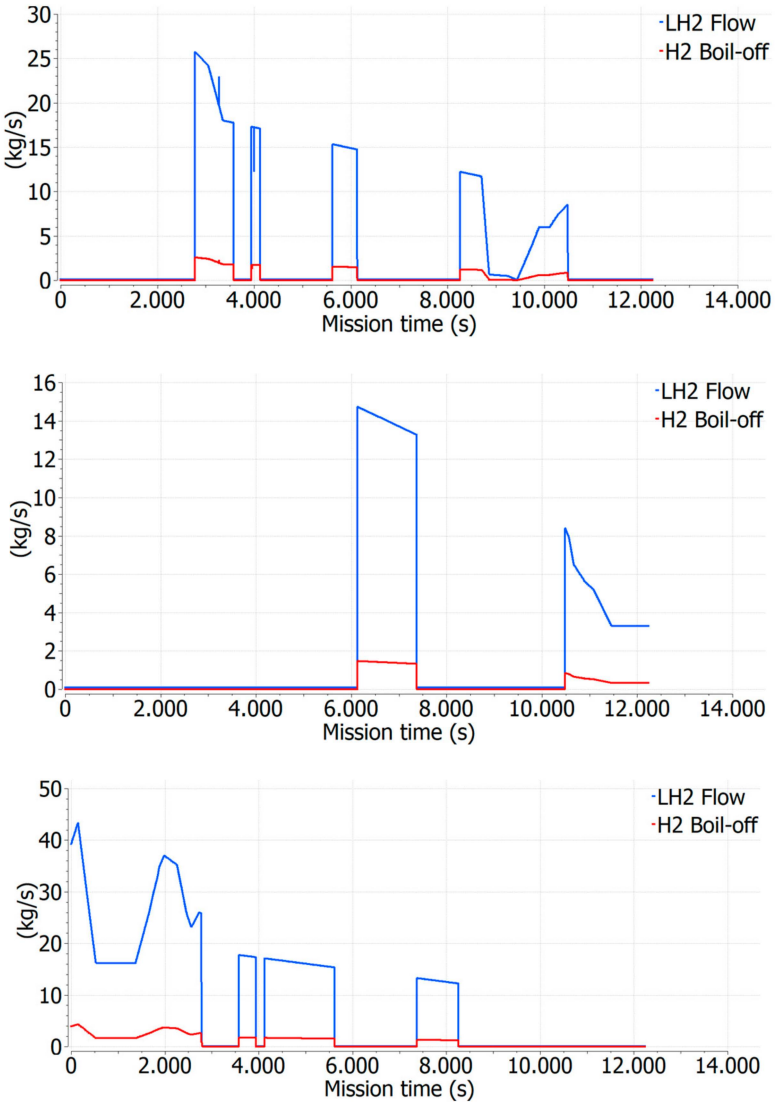


**Figure 10.** Propellant (blue) and boil-off (red) flows to feed TMS modules (module 1 to module 3).

The boil-off rate follows the same concept with the aforementioned ratio. It is worth highlighting again that this study only focuses on the powerplant side, with the hypotheses on insulation layers and passive thermal management layout of tank compartments previously discussed. The detailed derivation of the thermal equilibrium across the aeroshell contributing to the generation of the boil-off flow, as well as to keep the coolant flow within acceptable temperature, will require further assessments. The need for considering active solutions, such as the transpiration cooling techniques practically adopted for high-speed aircraft [27] or studied within advanced research associated with thermal management technologies [28] shall be carefully evaluated on a second iteration of this work. Additionally, dedicated intermediate cycles can be introduced in case the primary coolant flow cannot be maintained within reasonable temperature limits. In this case, as also shown in Section 2, a thorough analysis of the energy required for the system to work would be mandatory.

#### 4.2.4. Environmental Control System Interfaces

As already stated in Section 2, this work aims to explore the integration of the TMS with the environmental control system (ECS) as a unique example of a utility on-board system

interface (other than the propellant plant). As discussed in [4], the ECS architecture features a bleed-less layout, using an open-loop air cycle, capturing firstly ram-air from the main intake (not from the engines). Then, the flow is preliminarily managed, in terms of pressure and temperature, through electrical dedicated compressors. A bootstrap subfreezing cold air unit (CAU) architecture (Figure 11) allows for regulating the flow for cabin environment injection and managing the residual thermal loads impacting the passenger compartment, as well as guaranteeing breathable air values (in terms of clean incoming airflow).

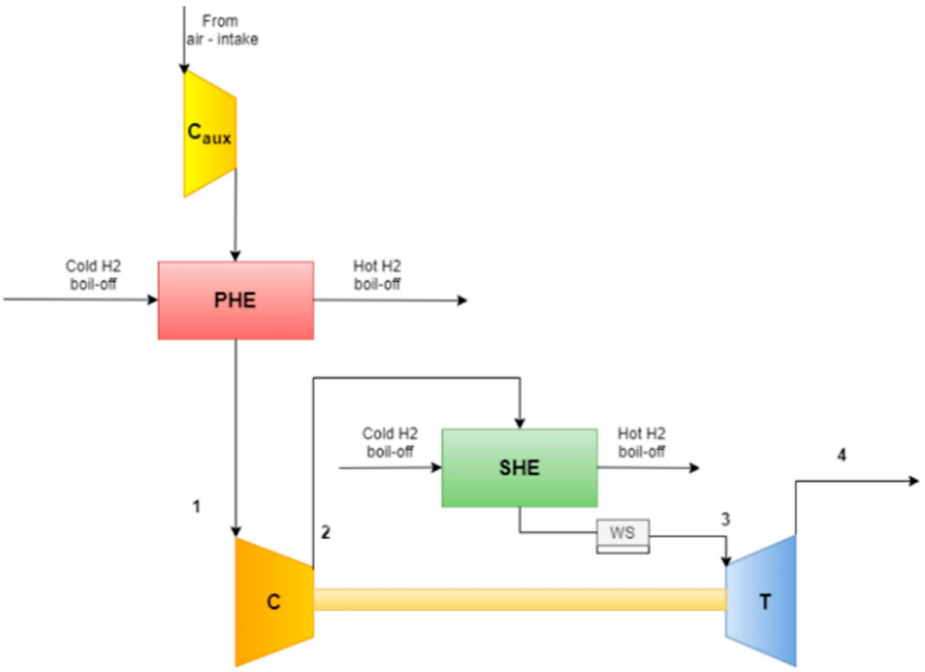


**Figure 11.** Cold air unit architecture [4].

The CAU has two exchangers to (i) reduce ram air temperature before entering the air cycle machine (ACM) and (ii) regulate processed air temperature before expansion in the ACM turbine. The exchangers make use of hydrogen boil-off as the main cooling means, using the flow rate previously assumed and coming from the tanks. The overall air flow to be managed by the ECS is around 14–22 kg/s for the whole set of cabin compartments, while the temperature levels of the flows are reported in Table 1 (used for sizing).

**Table 1.** ECS flow characterization (air).

| Station | Temperature [K] | Pressure [MPa] |
|---|---|---|
| 0–intake | 200–720 | 0.02–0.08 |
| 1 | 417 | 0.13 |
| 2 | 564 | 0.50 |
| 3 | 462 | 0.48 |
| 4 | 295 | 0.1 |

### *4.3. System Modeling*

The TMS concept was modeled within the EcosimPro 6.2 environment using the European Space Propulsion Systems Simulation library (ESPSS) 3.3.0 and, particularly, its steady subset of components [29]. For what concerns physical breakdown estimation as a function of operating parameters, the original correlations of ESPSS 3.3.0 [29] were enriched in order to obtain the mass and volumes of the overall TMS, while original performance and

dynamic equations (embedded within the libraries) were adopted for overall simulation, as described hereafter.

The EcosimPro environment was conceived to host an object-oriented coding (based on proprietary EL code), which enables the abstraction of a component behavior into abstract components. This offers the possibility of customizing the desired set of elements and the schematic itself, using inheritance and aggregation properties (to re-use or couple pre-defined algorithms, with the option of including new formulations). For the purpose of this analysis, the steady library of ESPSS was used, aiming to perform the design of the system, thus favoring the adoption of the built-in "design mode" of the different components, containing the design conditions as part of the input data and producing as output the sizing of the elements (mainly turbomachinery components). This approach was possible since the steady library contains a complete set of components (such as pumps, compressors, turbines, tanks, etc. . . . ) for the direct calculation of steady performance, benefiting from the simplified format of the equations from the same components provided within transient libraries. The fluids considered for the analysis came from the tool database and included real hydrogen as well as perfect air mixture. For what concerned the real fluids data and properties, the formulation used tables from the Reference Fluid Thermodynamic and Transport Properties Database (REFPROP 9.0) [30] coming from the US National Institute of Standards & Technology (NIST), enabling data interpolation when needed and extrapolation in case of values beyond the available ranges. On the other hand, perfect gas properties were computed according to the NASA CEA model [31]. Within transient libraries, there was a specific topology with which the components were coupled, since both capacitive and resistive elements were defined: capacitive components integrate mass and energy conservation equations so that thermodynamic functions embedded within the code can be used to calculate the complete state of the fluid; resistive components calculate explicitly the mass flows between capacitive elements to complete the equations set. However, the steady library is much simpler and a direct connection of elements of whatsoever type is allowed, also considering that the system of equations represents a steady state, not including time derivatives. The components included within the model were: tanks, pumps, compressors, turbines, cooling jackets and heat exchangers, as well as thermal interfaces and topological connections, such as junctions, which were used to impose mass flow values and thermal boundaries. A short description of the components is reported hereafter.

Steady tank components provided inlet boundary conditions to the schematic in terms of temperature and pressure. The component was also enriched with the possibility of computing the related mass, for both spherical (built-in) and cylindrical shapes (circular or elliptical section), with the evaluation of structural and insulation contributions. This was possible when operational variables (pressure of the compartments, temperature of the interfaces, tank materials and geometry) were provided, together with thicknesses (structural—hypothesized by user consistently with pressure, insulation—computed according to [26]). The model was based on the evaluation of thin shell compartment mass, considering structural and insulation contribution separately, as well as perfect cylindrical- or spherical-shape shells (tank ends were also considered in case cylindrical shape was concerned).

The pump components simulated machines for liquid pumping in steady conditions. They were parametrized with dimensionless characteristic curves and variables for several types of machines (e.g., specific speeds). These components incorporated the mass, energy and momentum equations in a steady regime. Then, depending on the boundary conditions, i.e., specific speed or mass flow, it was possible to compute the unknown variables by means of the definition reported in (2).

$$N_s = \frac{n\sqrt{Q/n_p}}{(H/n_s)^{0.75}} \tag{2}$$

where

$N_s$ is the specific speed;
$n$ is the actual rotational speed [rpm];
$Q$ is the volumetric flow rate [$m^3/s$];
$n_p$, $n_s$ are the number of parallel and serial stages of the pump, respectively;
$H$ is the pump head [m], defined as in (3)

$$H = \frac{p_{out} - p_{in}}{g\rho_{fuel}} \tag{3}$$

with

$p_{out}$, $p_{in}$ as the outlet and inlet pressure [Pa];
$g$ as gravity acceleration [$m/s^2$].

Considering a pressure differential within the machine, and a computed/imposed mass flow, it was also possible to evaluate torque (4), power (5) and enthalpy rise (6).

$$T = \dot{m}(p_{out} - p_{in}) / (\rho_{fuel}\eta\omega) \tag{4}$$

$$P = \dot{m}(p_{out} - p_{in}) / (\rho_{fuel}\eta) \tag{5}$$

$$dh = (p_{out} - p_{in}) / (\rho_{fuel}\eta) \tag{6}$$

where

$\dot{m}$ is the mass flow rate [kg/s];
$\omega$ is rotational speed [rad/s];
$\eta$ is the isentropic efficiency.

Evolution of fluid variables at the outlet were also computed according to the pump type (centrifugal, mixed, axial) depending on boundary conditions and specific performance. Additionally, in this case, mass breakdown formulations were added according to the models provided in [32,33] for turbopumps and in [34] for what concerned electrical pumps.

A similar approach was also used for the compressor and turbine components, with different maps taking into account characteristic blade-axe angle and inter-blade flow area, as well as overall pressure ratio (that could be selected also as a fixed constraint). Still, the components represented steady versions of the more extensive transient ones, so they incorporated mass, energy and momentum equations. They computed, as output, fluid variable evolution, as well as machine power demand/production. Mass estimation was in this case provided by [32,35].

The cooling jacket component represented a regenerative circuit for a specified chamber, embedding a 1D geometry (equivalent 1D wall around the channels) for which fluid and wall temperatures, as well as pressure losses and heat exchange coefficient, were physically calculated. A co-flow component was selected for simplicity. Depending on the position of the jacket, different fluid nodes could be specified, being connected to either nozzle or combustor interfaces. Specific tables could be used to perform a parametrization of the geometry in terms of diameter-to-length ratios, while material could be specified. In this way, a number of channels were hypothesized and linked to the heat absorption capability of the assembly, considering, in this case, hydrogen flow and high-temperature metallic alloys in terms of case material. Heat exchange for each node was computed considering the fluid–cold wall interface (internal) (7) and cold wall–hot wall interface (external) (8) separately. Pressure drop could also be evaluated, while the wall temperature at the nozzle throat section could be set as the boundary (where applicable). Channels were hypothesized as squared channels with specified dimensions.

$$q_{int}(i) = h_c(i)\left(\frac{A(i)}{n_{ch}}\right)\left(T_{wcold}(i) - T_{fluid}(i)\right) \tag{7}$$

$$q_{ext}(i) = \left(T_{whot}(i) - T_{wcold}(i)\right)\left(\frac{k(i)}{t(i)}\right)A(i) \tag{8}$$

where at the $i$-th different nodes:

$q_{int}, q_{ext}$ are the thermal power exchanged between internal and external interfaces [W];
$h_c$ is the heat transfer coefficient [W/m$^2$K];
$T_{wcold}$, $T_{whot}$ are the internal and external wall temperatures, respectively [K];
$k$ is the wall conductivity [W/mK];
$t$ is the wall thickness [m];
$A$ is the wetted area for heat exchange [m$^2$];
$n_{ch}$ is the number of channels.

Mass estimation was performed by means of geometrical relationships, taking into account the parametrized shape of the jacket and the void fraction of the channels. The fluid was not considered within the mass breakdown.

The heat exchanger component used for the TMS model was a simple element based on the conservation of mass and energy, for which a particular heat exchange efficiency was imposed together with a pressure drop to each side of the streams channel. This pressure drop was defined as percentage of the inlet pressures. The heat balance provided in (9) was imposed.

$$\dot{m}_{hot}\left(h_{hot_{in}} - h_{hot_{out}}\right) = \dot{m}_{cold}\left(h_{cold_{out}} - h_{cold_{in}}\right) \tag{9}$$

where

$\dot{m}_{hot}$, $\dot{m}_{cold}$ are the mass flow rates of hot and cold fluids [kg/s];
$h_{hot_{in}}$, $h_{hot_{in}}$ are the enthalpy levels of incoming/outgoing hot fluid [J/kg];
$h_{cold_{out}}$, $h_{cold_{in}}$ are the enthalpy levels of outgoing/incoming cold fluid [J/kg].

With the heat exchange efficiency defined in (10), depending on the known temperatures and specific heats (11), (12) it was possible to derive the evolution of the desired outputs for fixed mass flows.

$$\eta_{th} = \frac{\dot{m}_{hot}\left(h_{hot_{in}} - h_{hot_{out}}\right)}{\min\left(\dot{m}_{hot}c_{p_{hot}}, \dot{m}_{cold}c_{p_{cold}}\right)\left(T_{hot_{in}} - T_{cold_{in}}\right)} \tag{10}$$

$$c_{p_{hot}} = \frac{h_{hot_{out}} - h_{hot_{in}}}{T_{hot_{out}} - T_{hot_{in}}} \tag{11}$$

$$c_{p_{cold}} = \frac{h_{cold_{out}} - h_{cold_{in}}}{T_{cold_{out}} - T_{cold_{in}}} \tag{12}$$

where

$c_{p_{hot}}$, $c_{p_{cold}}$ are specific heats for hot and cold fluids, respectively [J/kgK];
$T_{hot_{in}}$, $T_{hot_{out}}$ are inlet and outlet temperatures of hot fluid [K];
$T_{cold_{in}}$, $T_{cold_{out}}$ are inlet and outlet temperatures of cold fluid [K].

Mass estimation in this case was not available since the component did not include material/geometrical properties out of the box.

The global TMS model (Figure 12) was implemented and then subdivided into three modules in order to simplify the simulation process and meet the module breakdown envisaged during the design process.

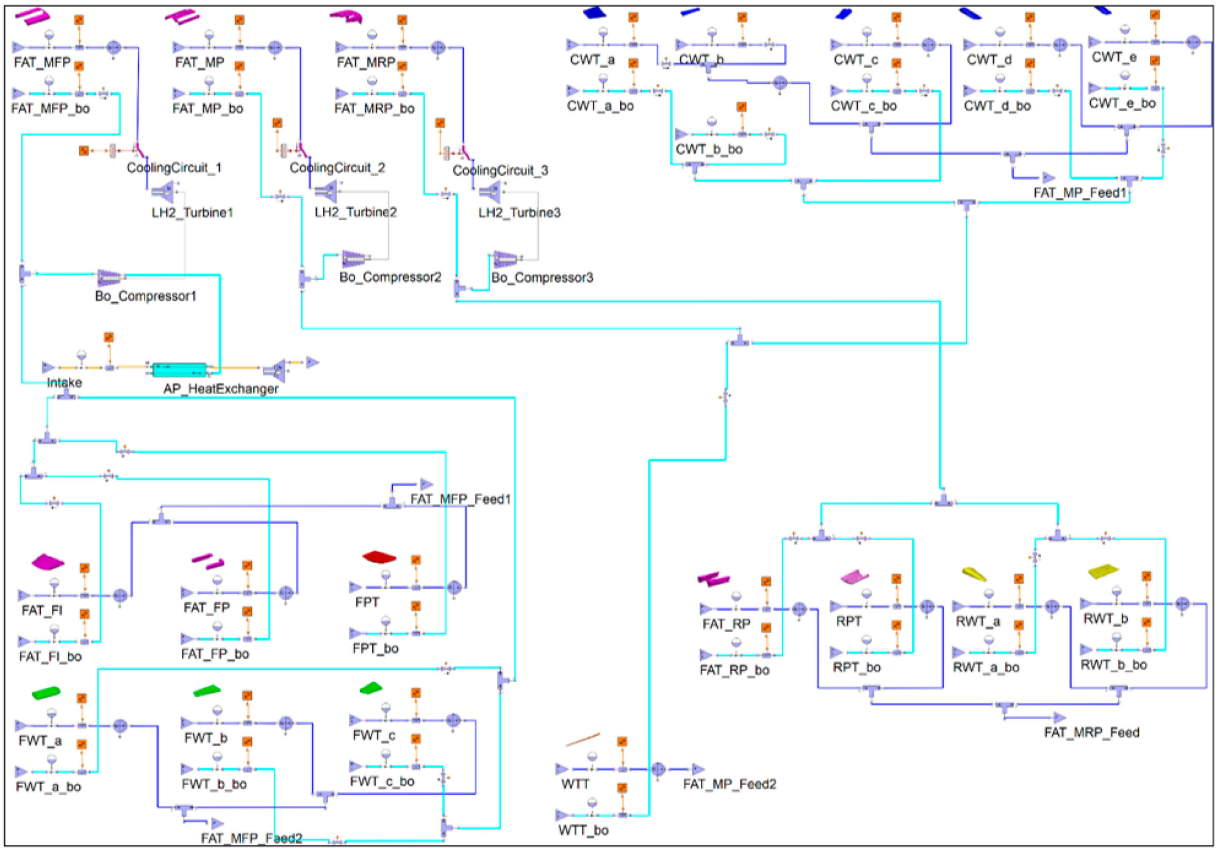


**Figure 12.** Overall thermal management system model in EcosimPro.

The model was conceived to simulate the entire mission, including as input the propellant mass flow, boil-off mass flow, airflow to be managed within the ECS and thermal flux coming from powerplant as function of time. LH2 circuits (blue) were conceived in order to convey LH2 from auxiliary tanks to primary tanks through electrical pumps. Then, a primary turbopump drove the flow to the regenerative cooling (flowing within the cooling jacket and then expanding within the turbine). On the other hand, boil-off circuits (cyan) were designed to connect auxiliary tanks and primary tanks to the overall collector, which was located before the compressor of each module. Then, the flow was compressed and could be used as the coolant means for different users (ECS heat exchanger is shown in this case). The boil-off compressor was physically connected to the LH2 turbine. Additionally, a short airflow circuit (orange) simulated the ECS incoming flow, from the outlet of the cold air unit (CAU) compressor to the cabin. Tank inlet conditions were specified depending on the mission phase, so that the outlet pressure of auxiliary tanks was the same pressure as within primary tanks (until they had fluid to be used within the cycle). This was reasonable considering that the boil-off created within the compartments is directly conveyed to the related compression cycle, not influencing in a noticeable way the internal pressure of the tanks. The outlet ports of LH2 turbines were kept in the conditions specified in Section 4.2.3, as well as the boil-off line outlet, while cabin pressure is specified in Table 1.

Each module was independent. This simplified the simulation campaign (Section 4.4), since each one could be simulated as a stand-alone, but results were managed during post-processing. In fact, when the module was not active, the assembly was in a sort of stand-by mode, not contributing to thermal management and power generation (there was no flow within the pipes and turbomachines were not active).

The first module (Figure 12 left side) included the front assembly, which was connected to the front additional tank—middle-front part (FAT—MFP) that acts as the primary tank (top purple compartment in Figure 13). Additionally, the related auxiliary tanks (FAT—

FI, FAT—FP, FPT and FWT modules) were included, as expected from the depletion strategy and propellant subsystem architecture described in Figures 5 and 7 (purple, red and green compartments in Figure 14, in the order they appear) [20]. Connection to the regenerative cycle, through the cooling jacket of the powerplant, was granted by the dedicated component. Moreover, the basic ECS elements were introduced. Notably, the upper part of the schematic (Figure 13) included the connection with the related primary tank (FAT-MFP), in terms of LH2 and boil-off lines, together with the regenerative cooling cycle and boil-off compression.

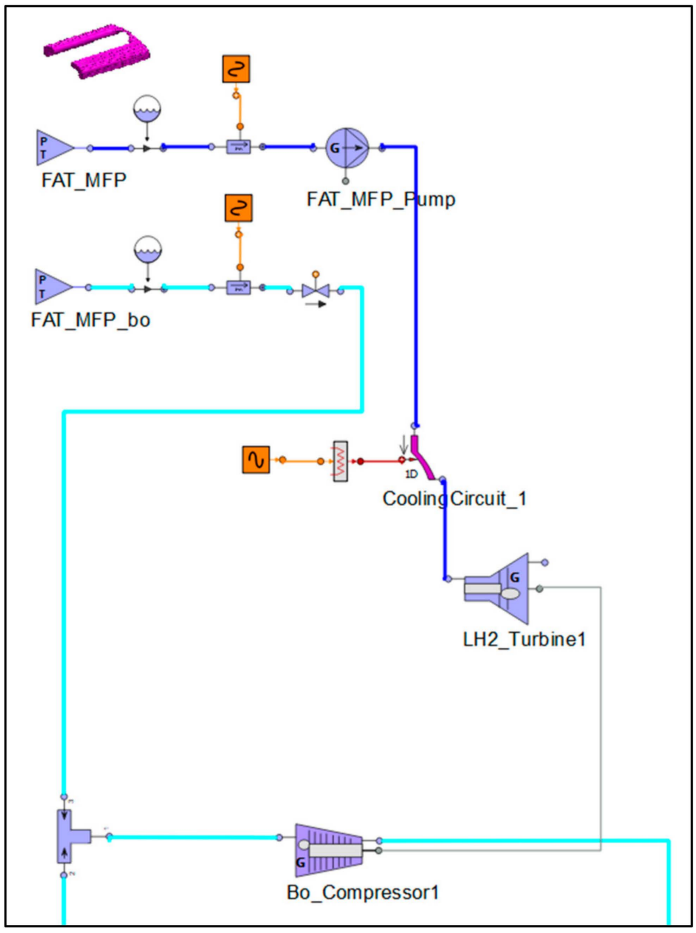


**Figure 13.** Front module, detail of primary tanks and turbomachinery.

The mass flow of both LH2 and boil-off (Figure 10, first row) was imposed following the depletion sequence analysis performed in [20] through proper control blocks (orange in the schematic). The same applies to the thermal power provided to the cooling jacket (Section 4.2.1). Similarly, this approach held also for the auxiliary tanks (Figure 14), with the difference that the outlet line of LH2 was mathematically connected to the overall flow exiting from the primary tank (not shown in the schematic). The boil-off line was physically connected to the compressor (the boil-off was not mixed inside the primary tank but it was connected directly to the cycle). Additionally, the ECS interface was introduced in order to simulate the segment of the circuit from the CAU compressor outlet up to the cabin, including the boil-off-based heat exchanger and airflow turbine (Figure 15).

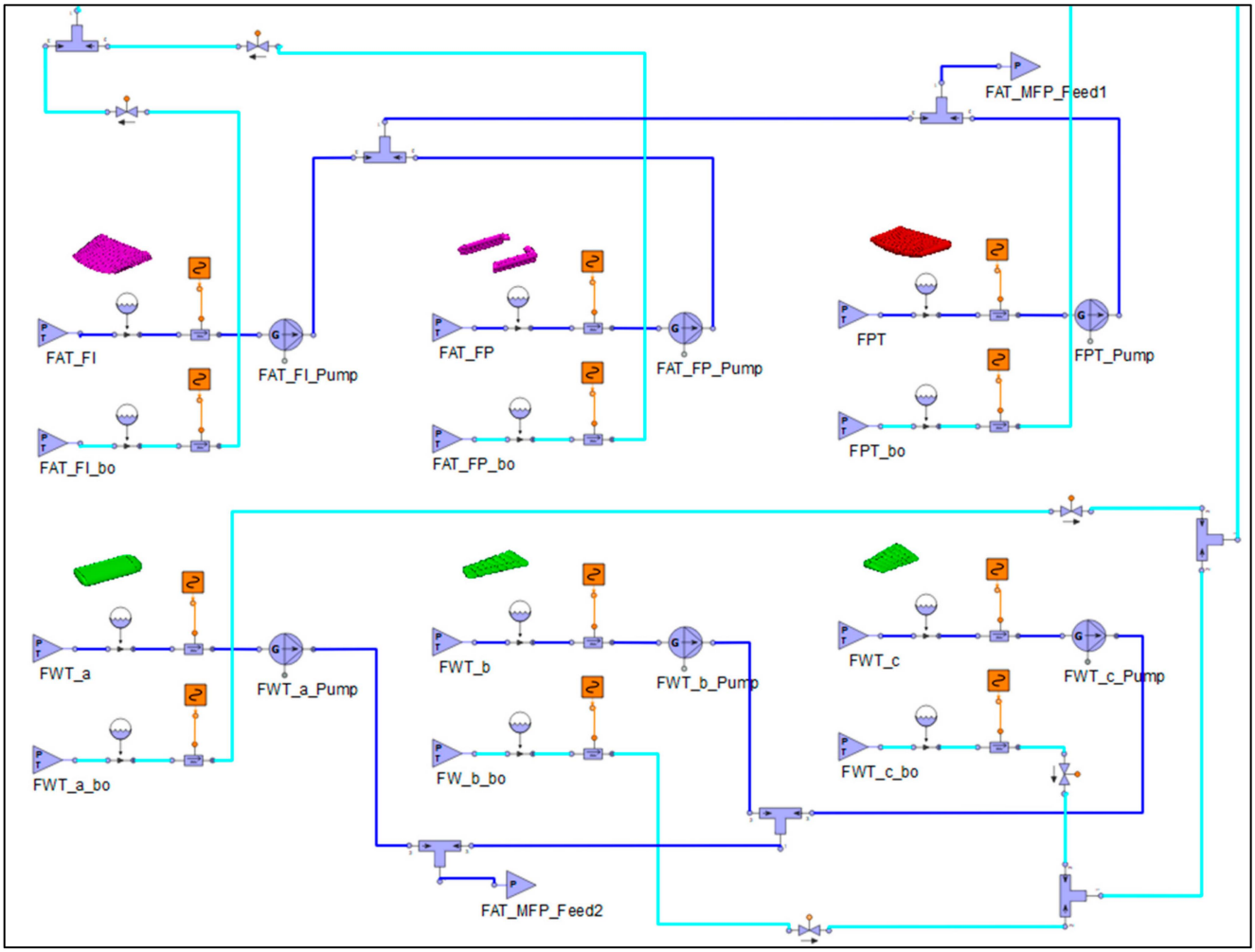


**Figure 14.** Front module, detail of auxiliary tanks.

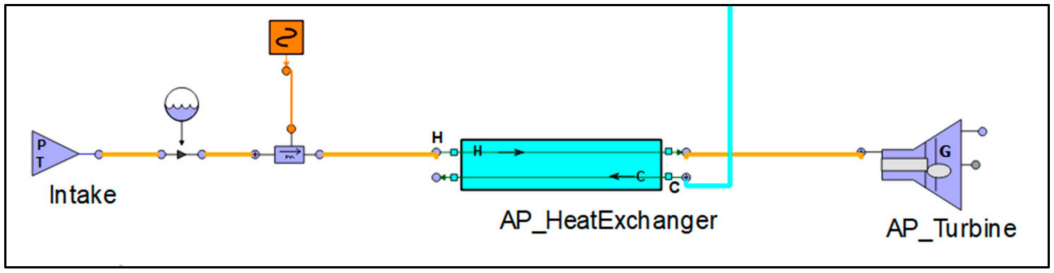


**Figure 15.** Front module, detail of ECS interface.

This rationale was also applied to the second module (middle TMS module) as well as the third one (rear module). For the second module, the primary tank was the FAT-middle part (FAT-MP), while auxiliary tanks were the center wing tank (CWT) and the wing tip tank (WTT) (see Figure 7, second picture). The same hypotheses on the routings of LH2 and the boil-off circuits applied, even if these were referred to the middle module only. Where possible, the different elements (such as pumps, compressors, turbines etc. . . . ) were kept equal in terms of performance. As far as the third module was concerned, the primary tank was the FAT—middle-rear part (FAT-MRP), while auxiliary tanks were the FAT-rear part (FAT-RP), rear pillow tank (RPT) and rear wing tank (RWT) (see Figure 7, last picture).

### *4.4. Simulation and Results*

A dedicated simulation was set up for the reference mission described in Section 3, taking into account the prescriptions discussed in Section 4.2 in terms of main interfaces and constraints to the system. As described in Section 4.1, the focus of the simulation was limited to the analysis of main turbomachinery input/output of the modules, together with the assessment of regeneration capability of the cooling jacket, with an eye on temperature levels reached, as well as to extra power generation opportunities. The three modules had different working sequences along the profiles since they were linked to the depletion sequence, i.e., the presence of LH2 fluid within the delivery lines. Thus, for what concerned the cooling jacket and the power generation results, it was more reasonable to assess the global picture of the complete system, where the three modules were covering alternatively different phases, according to Table 2. In this case, green rows identify first module activation, while yellow and blue ones are related to modules 2 and 3, respectively. On the other hand, individual turbomachine performance can be assessed by looking at the separated modules.

**Table 2.** Reference phases in which the different modules are active (green for module 1, yellow for module 2 and blue for module 3).

| Mission Time | Mission Phase | Reference Altitude | Reference Mach |
|---|---|---|---|
| 0–2777 | T/O—subsonic/supersonic/h climb | 0–28,800 | 0.3–6.35 |
| 2778–3572 | Hypersonic climb—hypersonic cruise | 28,800–32,700 | 6.35–8 |
| 3573–3941 | Hypersonic cruise | 32,700–33,400 | 8 |
| 3942–4122 | Hypersonic cruise | 33,400 | 8 |
| 4123–5618 | Hypersonic cruise | 33,400–34,000 | 8 |
| 5619–6131 | Hypersonic cruise | 34,000–34,200 | 8 |
| 6132–7374 | Hypersonic cruise | 34,200–34,700 | 8 |
| 7375–8254 | Hypersonic cruise | 34,700–35,000 | 8 |
| 8255–10,487 | Hypersonic cruise—hypersonic/supersonic descent | 35,000–18,700 | 8–1.2 |
| 10,488–12,238 | Supersonic/subsonic descent—approach–landing | 18,700–0 | 1.2–0.3 |

The simulation was performed using an implicit differential algebraic solver (IDAS) with a tolerance of $1 \times 10^{-6}$, producing outputs every 10 s with reference to the mission time.

Pressure and temperature trends across the boil-off compressor for the three modules are reported in Figure 16.

Only relevant time domains are shown (i.e., time frame for which the specific module is active). Pressures and temperatures appeared acceptable, even if some spikes could be noticed at specific instants, mainly due to numerical issues associated with module activation/de-activation.

Similar trends are reproduced in Figure 17 for the hydrogen turbine.

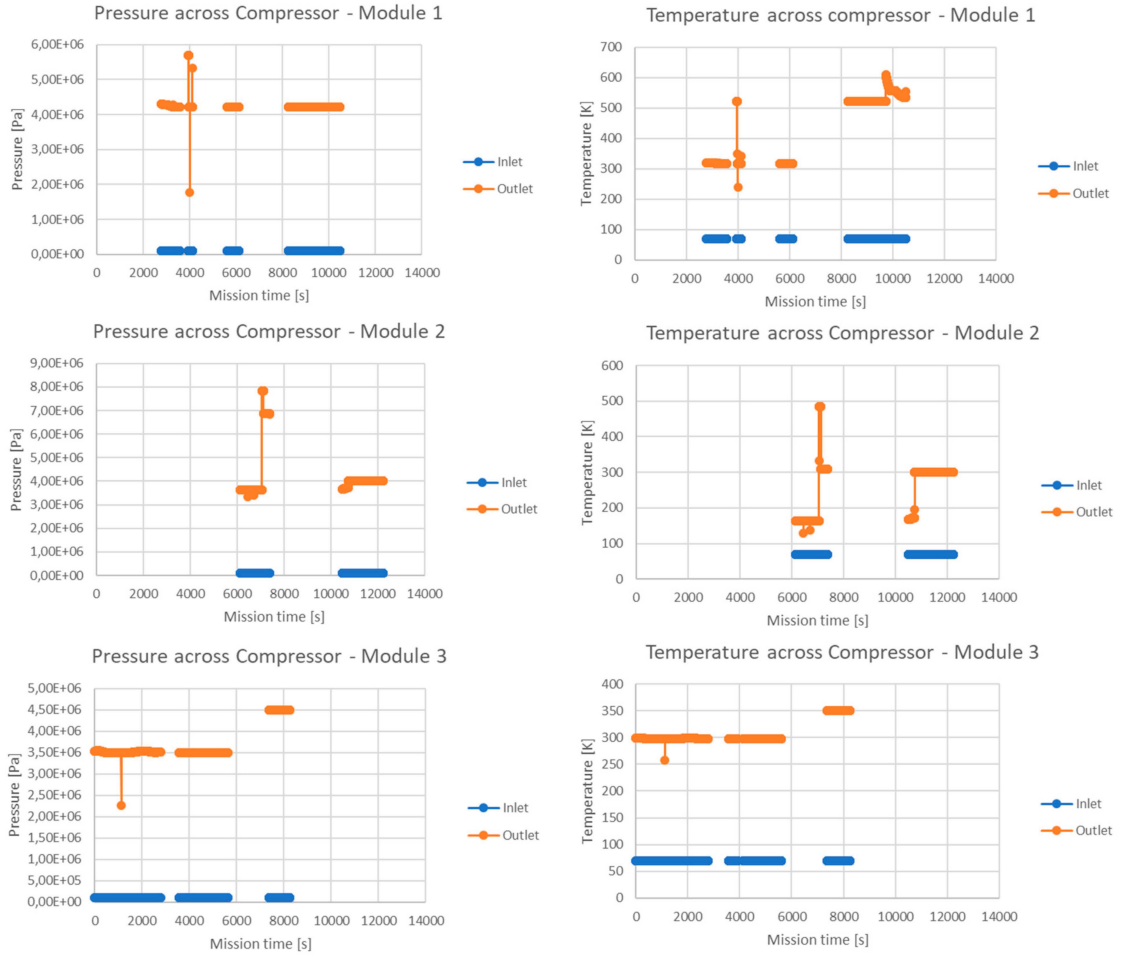


**Figure 16.** Pressure and temperature trends across boil-off compressors for the three TMS modules.

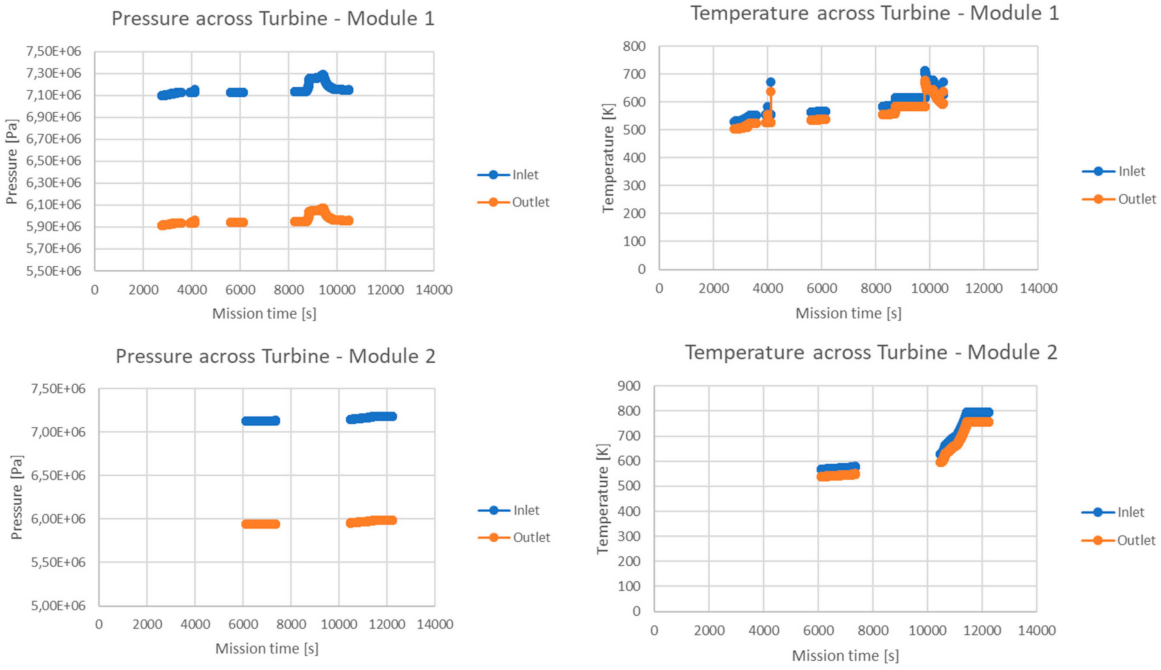


**Figure 17.** *Cont.*

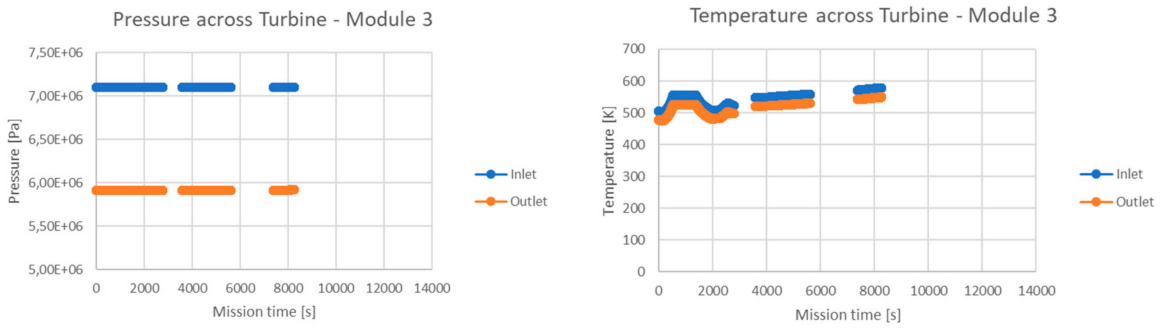


**Figure 17.** Pressure and temperature trends across hydrogen turbine for the three TMS modules.

The outlet of the air pack turbine was basically stable at 295 K and 0.1 MPa for cabin air injection. However, sea level pressure within the cabin may not be the best option considering the altitude of the cruise (high structural load), so additional analyses may be required to better control this value.

Pressure and temperature trends across the main cooling jacket are reported in (Figure 18). In general, temperature values remained within the expected limits. However, the temperature of the combustor–nozzle assembly monotonically increased, thus updates to the jacket configuration and parameters may be required to keep the value as steady as possible (also considering operational procedures at landing to make the airframe accessible). Additionally, pressure loss within the cooling jacket appeared underestimated, since the outlet value was still considerably high (around 7 MPa).

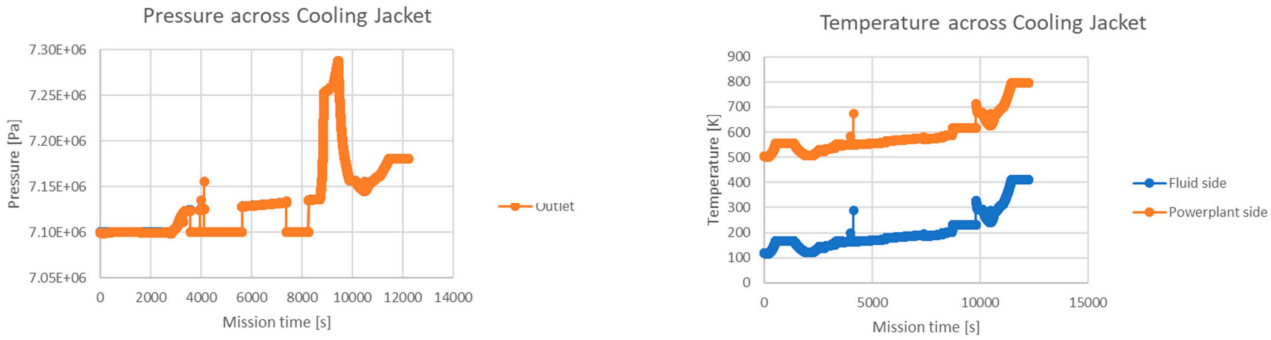


**Figure 18.** Pressure and temperature trends within the cooling jacket.

Overall, the power breakdown of the three modules of the system is reported in Figure 19.

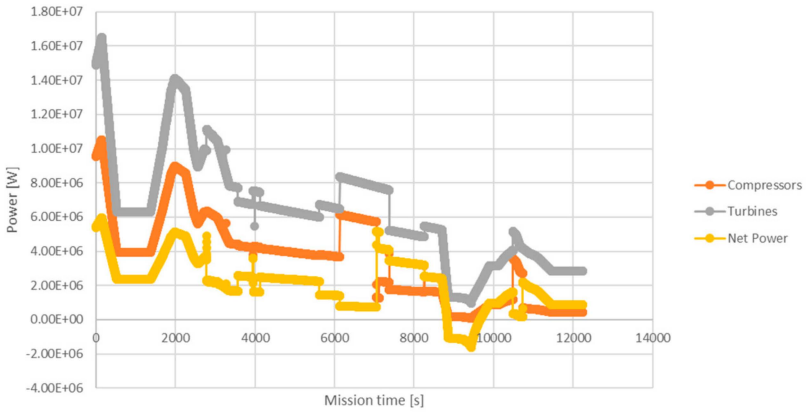


**Figure 19.** Overall secondary power generation trend.

The results appear satisfying for both individual modules and global trends, even if power generation may encounter a critical region between 8500–10,000 s of the mission, where the actual power consumed by TMS utilities is higher than the one produced. This is mainly due to the fact that, during descent, the powerplant operates at idle conditions, providing a low mass flow rate of hydrogen to the system. The maximum peak of secondary power generation was around 6 MW, but the negative peak (−1.8 MW) was also considerable. In general, average power generation was in line with vehicle demands (also considering that during ATR engines operation additional generators can be used), but the descent phase shall be assessed carefully to avoid such a big power differential.

According to the models used for the determination of physical breakdown of the system, as briefly recalled in Section 4.3, the mass and volume results for the main active elements are reported in Table 3.

**Table 3.** Mass and volume breakdown for active elements of the TMS.

| Element | Number | Total Mass [kg] | Total Volume [$m^3$] |
|---|---|---|---|
| Feed turbopumps | 6 | 1100 | 0.20 |
| Electrical transfer pumps | 40 | 870 | 0.15 |
| Boil-off compressors | 3 | 750 | 0.23 |
| Hydrogen turbines | 3 | 450 | 0.29 |

Please notice that pump assemblies were shared with the propellant system. The related number was associated with propellant system architecture, as described in [20]. Active assemblies of TMS had a global mass of 3170 kg and an overall volume of 0.87 $m^3$ (fittings, connections, etc., were not included in the volume breakdown). An additional mass of at least 360 kg should be taken into account for the cooling jacket. A total number of 20 modules were considered for the combustor, while 50 modules were selected for the nozzle, with the dimensions reported in Section 4.2.2, considering high-temperature metallic alloys.

## 5. Conclusions and Future Works

This paper introduces the concept of a thermal management system (TMS) with integrated on-board power generation capabilities for a Mach 8 hypersonic aircraft powered by liquid hydrogen (LH2), as assessed within the EU-funded STRATOFLY (STRATOspheric FLYing opportunities for high-speed propulsion concepts) Project. The TMS concept described in the paper makes benefit of the connection between the propellant storage and distribution systems of the aircraft to exploit hydrogen vapors and liquid flow as means to drive a thermodynamic cycle able, on one side, to ensure engine feed and thermal control of powerplant and the cabin environment, while providing, on the other hand, the necessary power for other on-board systems and utilities. Assumptions on TMS interfaces with other systems and the vehicle itself are provided, together with involved fluid mass flows for both vapor and liquid hydrogen. The modeling rationale that led to the implementation of a system schematic within the EcosimPro platform is presented. A simulation was performed for the different modules of the TMS to assess the main operating variables of the turbomachines, as well as global thermal management and power generation capability. The results appear promising, since the performance of the turbomachines seems in line with typical ranges of applications, and the thermal control of the main combustion chamber, as well as the nozzle of the powerplant assembly, was effective, maintaining temperature below 820 K thanks to dedicated regenerative cooling. Power generation capabilities were also remarkable. Still, a better understanding of the implemented cycle may be beneficial to limit even more the temperature of the powerplant walls, as well as correct a critical loss of power generation during descent phases. In fact, even if a peak of about 6 MW of secondary power can be provided during cycle operation, there is a deficit in produced power while powerplant operation is in the idle

mode. Additionally, additional focus on the environmental control system (ECS) operation logic may allow for better tuning of airflow injection pressure within the cabin, which for the purpose of this analysis was kept at 0.1 MPa. Overall, the mass of considered TMS elements was around 3530 kg. Future works shall then focus on these areas, also considering potential updates of the cycle, with additional simulations to validate this concept. In addition, updates to the mission itself may lead to different operating modes because of the connection with the propellant system. So, as long as modifications to the depletion sequence are expected, the model shall be flexible enough to be consistent with the interface requirements. Ultimately, more detailed analysis on boil-off characteristics, in terms of pressure, temperatures and flow shall be performed in order to further assess the viability of the concept, particularly focusing on the flow generation capability as well as the temperature evolution of the fluid throughout the mission.

**Author Contributions:** Conceptualization, D.F. and N.V.; methodology, D.F. and N.V.; software, D.F.; validation, D.F. and N.V.; formal analysis, D.F. and N.V.; investigation, D.F.; resources, D.F. and N.V.; data curation, D.F.; writing—original draft preparation, D.F.; writing—review and editing, N.V.; visualization, D.F.; supervision, N.V.; project administration, N.V.; funding acquisition, N.V. All authors have read and agreed to the published version of the manuscript.

**Funding:** This work was carried out in the framework of the Stratospheric Flying Opportunities for High-Speed Propulsion Concepts (STRATOFLY) Project, funded by the European Union's Horizon 2020 research and innovation program under Grant Agreement No 769246.

**Institutional Review Board Statement:** Not applicable.

**Informed Consent Statement:** Not applicable.

**Data Availability Statement:** The data associated to this work are not publicly available outside Project Consortium.

**Conflicts of Interest:** The authors declare no conflict of interest.

## Nomenclature

| | |
|---|---|
| ACM | Air cycle machine |
| ACN | Active cooling networks |
| ATR | Air turbo rocket |
| CAU | Cold air unit |
| CAV | Cruise and acceleration vehicle |
| CBC | Closed Brayton cycle |
| CFD | Computational fluid dynamics |
| CMC | Ceramic matrix composite |
| CoG | Center of gravity |
| CRB | Closed recuperative Brayton cycle |
| CWT | Center wing tank |
| DMR | Dual-mode ramjet |
| ECS | Environmental control system |
| FAT-FI | Front additional tank-front intake |
| FAT-FP | Front additional tank-front part |
| FAT-MFP | Front additional tank-middle front part |
| FAT-MP | Front additional tank-middle part |
| FAT-MRP | Front additional tank-middle rear part |
| FAT-RP | Front additional tank-rear part |

| | |
|---|---|
| FPT | Front pillow tank |
| FWT | Front wing tank |
| LH2 | Liquid hydrogen |
| MTOW | Maximum take-off weight |
| PCHE | Printed circuit heat exchanger |
| PTMS | Power and thermal management system |
| RPT | Rear pillow tank |
| RWT | Rear wing tank |
| SCO2 | Supercritical carbon dioxide |
| TEG | Thermo-electric generator |
| TEMS | Thermal and energy management system |
| TMS | Thermal management system |
| TPS | Thermal Protection System |
| TRL | Technology Readiness Level |
| WTT | Wing tip tank |

## Symbols

| | |
|---|---|
| $A$ | Wetted area [$m^2$] |
| $c_{p_{hot}}$, $c_{p_{cold}}$ | Specific heats [J/kgK] |
| $g$ | Gravity acceleration [$ms^2$] |
| $h_c$ | Heat transfer coefficient [$W/m^2K$] |
| $h_{cold_{out}}$, $h_{cold_{in}}$, $h_{hot_{in}}$, $h_{hot_{in}}$ | Enthalpy levels [J/kg] |
| $h_{fuel}$ | Heat of vaporization [J/kg] |
| $H$ | Pump head [m] |
| $k, k_{ins}$ | Conductivity [W/(mK)] |
| $\dot{m}$, $\dot{m}_{hot}$, $\dot{m}_{cold}$ | Mass flow rates [kg/s] |
| $n$ | Rotational speed [rpm] |
| $n_{ch}$ | Number of channels |
| $n_p$, $n_s$ | Number of parallel and serial stages |
| $N_s$ | Specific speed |
| $p_{out}$, $p_{in}$ | Pressures [Pa] |
| $q_{int}$, $q_{ext}$ | Thermal power [W] |
| $Q$ | Volumetric flow rate [$m^3/s$] |
| $t$ | Wall thickness [m] |
| $t_{flight}$ | Flight time [s] |
| $T_{cold_{in}}$, $T_{cold_{out}}$, $T_{fluid}$, $T_{hot_{in}}$, $T_{hot_{out}}$, $T_{int}$, $T_{wcold}$, $T_{whot}$ | Temperatures [K] |
| $\rho_{fuel}$ | Density of propellant [$kgm^3$] |
| $\omega$ | Rotational speed [rad/s] |
| $\eta$ | Isentropic efficiency |

## References


1. Hirschel, E.H. *Basics of Aerothermodynamics*, 2nd ed.; Springer: Berlin/Heidelberg, Germany, 2015. [CrossRef]
2. Hirschel, E.H.; Weiland, C. *Selected Aero-Thermodynamic Design Problems of Hypersonic Flight Vehicles*; Springer: Berlin/Heidelberg, Germany, 2009. [CrossRef]
3. Fernandez Villace, V.; Steelant, J. The Thermal Paradox of Hypersonic Cruisers. In Proceedings of the 20th AIAA International Space Planes and Hypersonic Systems and Technologies Conference, Glasgow, UK, 6–9 July 2015. [CrossRef]
4. Viola, N.; Ferretto, D.; Fusaro, R.; Scigliano, R. Performance Assessment of an Integrated Environmental Control System of Civil Hypersonic Vehicles. *Aerospace* **2022**, *9*, 201. [CrossRef]
5. Qing, J.; Zhou, W.; Bao, W.; Yu, D. Thermodynamic analysis and parametric study of a closed Brayton cycle thermal management system for scramjet. *Int. J. Hydrogen Energy* **2010**, *35*, 356–364. [CrossRef]
6. Gou, J.J.; Chang, Y.; Yan, Z.-W.; Chen, B.; Gong, C.-L. The design of thermal management system for hypersonic launch vehicles based on active cooling networks. *Appl. Therm. Eng.* **2019**, *159*, 113938. [CrossRef]
7. Chen, W.; Wang, R.; Li, X.; Lu, S.; Fang, X. Study of the heat transfer design on an integrated thermal management system for hypersonic vehicles using supercritical nitrogen as expendable coolant. *Aerosp. Sci. Technol.* **2022**, *123*, 107440. [CrossRef]
8. Viola, N.; Roncioni, P.; Gori, O.; Fusaro, R. Aerodynamic Characterization of Hypersonic Transportation Systems and Its Impact on Mission Analysis. *Energies* **2021**, *14*, 3580. [CrossRef]

9. Balland, S.; Fernandez Villace, V.; Steelant, J. Thermal and Energy Management for Hypersonic Cruise Vehicles—Cycle Analysis. In Proceedings of the 20th AIAA International Space Planes and Hypersonic Systems and Technologies Conference, Glasgow, UK, 6–9 July 2015. [CrossRef]
10. Cheng, K.; Qin, J.; Sun, H.; Dang, C.; Zhang, S.; Liu, X.; Bao, W. Performance assessment of a closed-recuperative-Brayton-cycle based integrated system for power generation and engine cooling of hypersonic vehicle. *Aerosp. Sci. Technol.* **2019**, *87*, 278–288. [CrossRef]
11. Cheng, K.; Qin, J.; Sun, H.; Dang, C.; Zhang, S.; Liu, X.; Bao, W. Performance assessment of an integrated power generation and refrigeration system on hypersonic vehicles. *Aerosp. Sci. Technol.* **2019**, *89*, 192–203. [CrossRef]
12. Guo, L.; Pang, L.; Yang, X.; Zhao, J.; Desheng, M.A. A power and thermal management system for long endurance hypersonic vehicle. *Chin. J. Aeronaut.* **2022**, *36*, 29–40. [CrossRef]
13. Guo, L.; Pang, L.; Zhao, J.; Yang, X. Optimization of Power and Thermal Management System of Hypersonic Vehicle with Finite Heat Sink of Fuel. *Energies* **2022**, *15*, 5332. [CrossRef]
14. Viola, N.; Fusaro, R.; Gori, O.; Marini, M.; Roncioni, P.; Saccone, G.; Saracoglu, B.; Ispir, A.C.; Fureby, C.; Nilsson, T.; et al. Stratofly mr3—How to reduce the environmental impact of high-speed transportation. In Proceedings of the AIAA Scitech 2021 Forum, Virtual, 11–21 January 2021. [CrossRef]
15. Viola, N.; Fusaro, R.; Vercella, V. Technology roadmapping methodology for future hypersonic transportation systems. *Acta Astronaut.* **2022**, *195*, 430–444. [CrossRef]
16. Viscio, M.A.; Gargioli, E.; Hoffman, J.A.; Maggiore, P.; Messidoro, A.; Viola, N. Future space exploration: From reference scenario definition to key technologies roadmaps. In Proceedings of the 63rd International Astronautical Congress, Naples, Italy, 1–5 October 2012; pp. 9131–9145.
17. Steelant, J.; Varvill, R.; Defoort, S.; Hannemann, K.; Marini, M. Achievements Obtained for Sustained Hypersonic Flight within the LAPCAT-II Project. In Proceedings of the 20th AIAA International Space Planes and Hypersonic Systems and Technologies Conference, Glasgow, UK, 6–9 July 2015. [CrossRef]
18. Fusaro, R.; Ferretto, D.; Viola, N.; Scigliano, R.; De Simone, V.; Marini, M. Liquid Metals Heat-Pipe solution for hypersonic air-intake leading edge: Conceptual design, numerical analysis and verification. *Acta Astronaut.* **2022**, *197*, 336–352. [CrossRef]
19. Fusaro, R.; Ferretto, D.; Viola, N. Flight Control System Design and Sizing Methodology for hypersonic cruiser. In Proceedings of the AIAA Aviation Forum 2022, Chicago, IL, USA, 27 June–1 July 2022. [CrossRef]
20. Ferretto, D.; Fusaro, R.; Viola, N. Propellant subsystem design for hypersonic cruiser exploiting liquid hydrogen. In Proceedings of the AIAA Aviation Forum 2022, Chicago, IL, USA, 27 June–1 July 2022. [CrossRef]
21. Fusaro, R.; Vercella, V.; Ferretto, D.; Viola, N.; Steelant, J. Economic and environmental sustainability of liquid hydrogen fuel for hypersonic transportation systems. *CEAS Space J.* **2020**, *12*, 441–462. [CrossRef]
22. Hoelzen, J.; Silberhorn, D.; Bensmann, B.; Hanke-Rauschenbach, R. Hydrogen-powered aviation and ist reliance on green hydrogen infrastructure—Review and research gaps. *Int. J. Hydrogen Energy* **2022**, *47*, 3108–3130. [CrossRef]
23. Scigliano, R.; De Simone, V.; Fusaro, R.; Ferretto, D.; Maini, M.; Viola, N. Cooling system of STRATOFLY hypersonic vehicle: Conceptual design, numerical analysis and verification. In Proceedings of the 33rd Congress of the International Council of the Aeronautical Sciences, Stockholm, Sweden, 4–9 September 2022.
24. Fernandez Villace, V.; Paniagua, G.; Steelant, J. Installed performance evaluation of an air turbo-rocket expander engine. *Aerosp. Sci. Technol.* **2014**, *35*, 63–79. [CrossRef]
25. Goncalves, P.M.; Ispir, A.C.; Saracoglu, B.H. Development and optimization of a hypersonic civil aircraft propulsion plant with regenerator system. In Proceedings of the AIAA Propulsion and Energy 2019 Forum, Indianapolis, IN, USA, 19–22 August 2019. [CrossRef]
26. Ardema, M.D. *Solutions of Two Heat-Transfer Problems with Application to Hypersonic Cruise Aircraft*; NASA Technical Memorandum TM X-2025; NASA: Washington, DC, USA, 1970.
27. Irwin, K.S.; Andrews, W.H. *Summary of XB-70 Airplane Cockpit Environmental Data*; NASA Technical Report TN-D 5449; NASA: Washington, DC, USA, 1969.
28. Steelant, J. Achievement obtained on Aero-Thermal Loaded Materials for High-Speed Atmospheric Vehicles within ATLLAS. In Proceedings of the 16th AIAA International Space Planes and Hypersonic Systems and Technologies Conference, Bremen, Germany, 19–22 October 2009. [CrossRef]
29. Vilà, J.; Moral, J.; Fernandez Villace, V.; Steelant, J. An overview of the ESPSS Libraries: Latest Developments and Future. In Proceedings of the Space Propulsion Conference 2018, Seville, Spain, 14–18 May 2018.
30. Lemmon, E.W.; McLinden, M.O.; Hiber, L. *NIST Reference Fluid Thermodynamic and Transport Properties—REFPROP v9.0*; NIST: Gaithersburg, MD, USA, 2013.
31. Gordon, S.; McBride, B.J. *Computer Program for Calculation of Complex Chemical Equilibrium Compositions and Applications, Part I: Analysis*; NASA Lewis Research Center: Cleveland, OH, USA, 1994.
32. Fusaro, R.; Ferretto, D.; Viola, N.; Fernandez Villace, V.; Steelant, J. A methodology for preliminary sizing of a Thermal and Energy Management System for a hypersonic vehicle. *Aeronaut. J.* **2019**, *123*, 1508–1544. [CrossRef]
33. Tizon, J.M.; Roman, A. A mass model for Liquid Propellant Rocket Engines. In Proceedings of the 53rd AIAA-SAE-ASEE Joint Propulsion Conference, Atlanta, GA, USA, 10–12 July 2017. [CrossRef]

34. Rachov, P. *Electric Feed Systems for Liquid Propellant Rocket Engines*; Research Report; Buenos Aires University: Buenos Aires, Argentina, 2010. [CrossRef]
35. Nieman, D.; Schreurs, M. Design of an Integrated Thermal Protection and Energy Management System for Hypersonic Air-Breathing Vehicles. Master's Thesis, KU Leuven, Leuven, Belgium, 2021.